J. Fluid Mech. (1989), *vol.* 203, *pp.* 103–123
Printed in Great Britain

The relationship between surface-renewal and bursting motions in an open-channel flow

By SATORU KOMORI[1], YASUHIRO MURAKAMI[1] AND HIROMASA UEDA[2]

[1] Department of Chemical Engineering, Kyushu University, Hakozaki, Fukuoka 812, Japan

[2] Division of Atmospheric Environment, The National Institute for Environmental Studies, Tsukuba, Ibaraki 305, Japan

(Received 21 January 1988 and in revised form 14 November 1988)

Surface-renewal motions in the interfacial region below a gas–liquid interface were experimentally investigated in relation to bursting motions in the wall region. To estimate the frequency of the appearance of surface-renewal eddies, mass-transport experiments with methylene-blue solution, together with velocity measurements, were done in an open-channel flow. The instantaneous concentration of methylene-blue tracer emitted from a point source positioned in the buffer layer was measured at the free surface downstream from the source by an optical probe. Instantaneous streamwise velocity was measured using a laser-Doppler velocimeter at a position in the buffer region. Frequencies of both surface-renewal and bursting events were computed from these concentration and velocity signals using a conditional-averaging method. In order to clarify whether the surface-renewal eddies actually dominate mass transfer across the gas–liquid interface, gas-absorption experiments were added. Carbon dioxide was absorbed into the water flow across the calm free surface and its mass-transfer coefficient on the liquid side was measured under the same flow conditions as used in the above mass-transport experiments. The results show that the surface-renewal motions originate in the bursting motions which vigorously occur in the buffer region. That is, the decelerated fluid which is strongly lifted towards the outer layer by bursting almost always arrives at the free surface and renews the free surface. The frequency of the surface renewal, as well as the bursting frequency, is uniquely determined by the wall variables or the outer-flow variables and the Reynolds number. Mass transfer across the gas–liquid interface is dominated by the large-scale surface-renewal eddies, and the mass-transfer coefficient on the liquid side is proportional to the square-root of the surface-renewal frequency.

1. Introduction

The mechanism of turbulent heat and mass transfer across a gas–liquid interface (free surface) is of great practical interest in the areas of both engineering and geophysics. Such a scalar transfer can be seen in many industrial processes, including gas absorption, evaporation and many others. It is also related to environmental problems such as thermal and water pollution in rivers and oceans, and the recycling of heat and mass between the atmosphere and water. Usually the liquid flow below the gas flow is turbulent, and the resistance on the liquid side dominates the mass transfer across a gas–liquid interface when the Henry constant of the gas is not so small. Therefore the investigation of the turbulent structure on the liquid side near

the interface is of great importance in estimating the scalar transfer across the interface (Hunt 1984).

Komori *et al.* (1982*a*, 1988) measured the turbulence quantities in the interfacial region of a fully developed open-channel flow, and suggested that energy-containing (large-scale) eddies are extremely elongated longitudinally and laterally by the presence of the free surface and intermittently renew the free surface. Furthermore, they suggested that the large-scale surface-renewal eddies control the heat and mass transfer across the free surface on the liquid side, and presumed that the frequency of the appearance of surface-renewal eddies (hereinafter termed the surface-renewal frequency) is proportional to the mean velocity at the free surface. However, they could not account for both how the surface-renewal eddies are generated and how they affect the scalar transfer across a gas–liquid interface.

On the other hand, reviewing the much-published data that had been obtained in natural rivers with rough beds, Jackson (1976) suggested that the frequency of the renewal eddies or boils in the natural rivers may be almost proportional to the frequency of the appearance of bursting motions (hereinafter termed the bursting frequency), estimated from laboratory measurements. He also presumed that vigorous eddies ejected by bursting phenomena in the wall region may become surface-renewal eddies. However, Jackson's (1976) work was based only on observations of the frequency of boils in natural rivers. Moreover, the bursting frequencies in the rivers were estimated from the results of the laboratory experiments over a smooth wall. Since the extension of the experimental relation to natural rivers is questionable because of the complicated boundary conditions, e.g. rough beds and three-dimensional flows, Jackson (1976) could not propose a conclusive relation between the boils (surface-renewal motions) and the bursting motions themselves.

The purpose of this study is both to experimentally make clear the relationship between surface-renewal motions and bursting motions, and to show that the mass transfer across the gas–liquid interface is dominated by the large-scale surface-renewal motions. The present flow configuration was a fully developed open-channel flow under subcritical and turbulent conditions. A solution of methylene-blue was emitted as a tracer of a bursting motion from a point source located in the buffer region. The concentration of the methylene-blue convected by the bursting motion was measured at the free surface by a small optical probe, which could detect the surface-renewal motions. On the other hand, the bursting motions were detected by a laser-Doppler velocimeter from measurements of the streamwise velocity at a position located in the buffer region. To educe the frequencies of both the surface renewal and bursting from the above measurements of concentration and velocity, a conditional-averaging technique was used. Based on these frequencies, the generation mechanism of the surface-renewal eddies is discussed, relating it to the bursting motions. CO_2-absorption experiments were done under the same flow conditions. The mass-transfer rate of CO_2 was measured and the effects of the surface-renewal motions on the mass transfer across the free surface are discussed.

2. Experiments

2.1. *Flow arrangement*

The flow arrangement used was very similar to that used by Komori *et al.* (1982*a*, *b*), and only the main hydraulic parameters are presented here. The apparatus used was a glass open flume 7.6 m long, 0.5 m wide and 0.2 m deep, and fresh water with a

Run no.	Symbol	$\delta \times 10^2$ (m)	$U_{ave} \times 10^2$ (m s^{-1})	$u^* \times 10^2$ (m s^{-1})	Re	Fr
I	○	1.1	23.5	1.48	10000	0.711
II	●	2.9	9.7	0.61	10100	0.182
III	◒	3.1	18.3	1.06	20000	0.355
IV	◓	5.0	5.9	0.37	9800	0.083
V	△	5.1	11.9	0.69	20000	0.169
VI	▲	6.4	19.1	1.01	39000	0.242
VII	▽	7.0	13.8	0.75	30000	0.166
VIII	□	10.0	10.5	0.58	30100	0.107
IX	■	11.2	10.9	0.59	33700	0.104

TABLE 1. Flow parameters and symbols corresponding to experimental runs.

constant temperature was recirculated into it. The flow depth δ ranged from 0.011 m to 0.112 m, and so the aspect ratio was 4.4 to 45.5. The cross-sectional mean velocity U_{ave} ranged from 0.059 m/s to 0.235 m/s, so that the Reynolds number based on the hydraulic radius was 9800–33 700 and the hydraulic Froude number was 0.1–0.71. Therefore, the flow investigated was a turbulent flow under hydraulically subcritical conditions. The values of flow parameters used in this study are listed in table 1. A fully developed flow was established in the region beyond 3 m downstream from the inlet of the flume, which was confirmed by the measurements of both the mean velocity and root-mean-square value of the streamwise velocity fluctuation. Typical distributions of mean velocity and root-mean-square (r.m.s.) values of streamwise velocity fluctuations u' in a developed open-channel flow, normalized by inner and outer variables, are shown in figures 1 and 2. Here the friction velocity u^* was estimated from the mean velocity gradient in the immediate vicinity of the wall. The friction factors calculated from the friction velocity obeyed the Blasius formula well. These velocity distributions are in agreement with the measurements by Komori *et al.* (1982*a*) and Mizushina *et al.* (1978).

2.2. *Measurement and processing*

Figure 3 shows schematically the experimental instruments and data-acquisition system. To trace the large-scale eddy motions generated by bursting in the buffer region, a point source with diameter 0.0012 m was fixed at the centre of the flume ($z = 0$ and $x = 0$) in the fully developed region approximately 3–4 m downstream of the inlet of the flume and at the dimensionless height of $y^+ = 15$ in the buffer region near the wall. A 0.25 wt % aqueous solution of methylene-blue was emitted from the point source at a speed equal to the ambient-flow velocity. The instantaneous concentration of methylene-blue was measured using a small optical probe of 0.001 m in diameter at the free surface in the region downstream of the point source. A beam of visible light from a light-emitting diode (Sharp GL 51AR) passed from one fibre to the other through the fluid between the two ends. The optical length between the ends was 1 mm. The beam was then led to a photodiode (Sharp BS 112) through the second fibre, and the electric-current output was converted to a voltage proportional to concentration by a converter (Masatoyo MT-C.M.I.). The details of this optical probe are described in Komori *et al.* (1982*b*). In addition to a fixed point source, a second source was sometimes used in the preliminary experiments as described in §3.1.

The instantaneous streamwise velocity was measured using a laser-Doppler

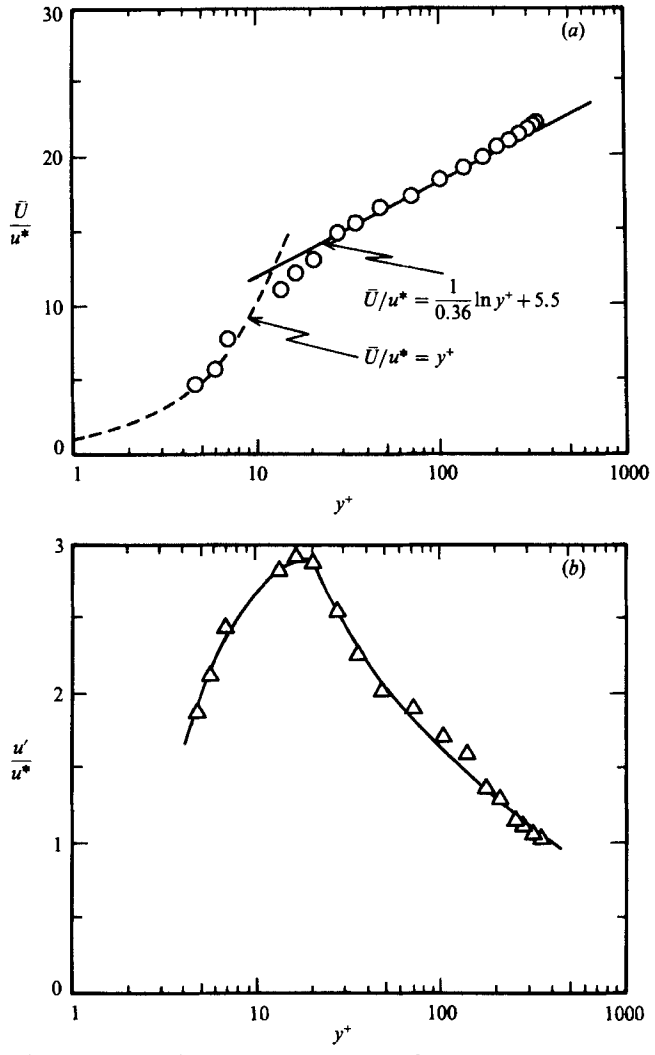

FIGURE 1. Typical distributions of (*a*) mean velocity and (*b*) root-mean-square values of streamwise velocity fluctuation, normalized by inner variables (run V). Lines show best-fit curves.

velocimeter (Dantec 55X System) to educe bursting motions generated in the buffer region. The accuracy of the velocity measurements has been verified in an earlier work (Komori & Ueda 1985). The measuring position was located at $y^+ = 15$, $z = 0$ and $x = 0$ in the fully developed region.

Both instantaneous concentration and velocity signals were transmitted directly into a digital recorder (TEAC DR-1000) and stored on a magnetic tape. The sampling interval and the sample size were 0.005 s and 120000, respectively. These digital signals were processed statistically by a digital computer. From these processed signals, frequencies of both surface-renewal and bursting events were counted using a conditional-averaging technique. The counting technique is presented in §3.

For the gas-absorption experiments, pure carbon dioxide (CO_2) at 20 °C was used, filling a rectangular hood at atmospheric pressure. The hood, made of polymethylemethacrylate (PMMA), was 1 m long, 0.3 m wide and 0.3 m high, and it lightly covered the free surface, as shown in figure 3. To minimize the blocking of the

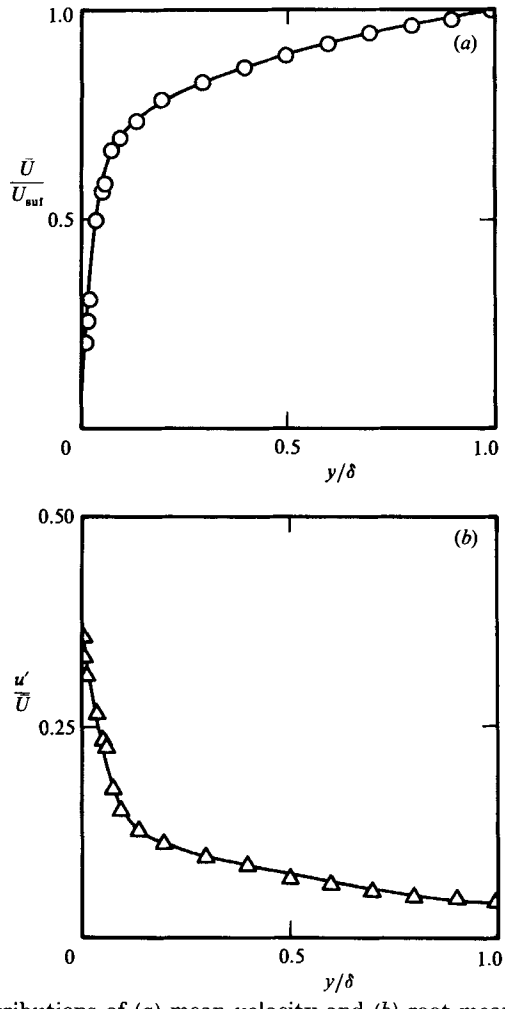

FIGURE 2. Typical distributions of (*a*) mean velocity and (*b*) root-mean-square values of streamwise velocity fluctuation, normalized by outer variables (run V). Lines show best-fit curves.

free surface flow by the hood, those parts of it in contact with the free surface were tapered to 0.0005 m thickness, and the hood was located at the central part of the flume to avoid the sidewall effects of the flume. The rate of absorption was measured with a soap-film meter and the absorption coefficient on the liquid side was estimated from the rate.

3. Counting technique for frequencies of surface renewal and bursting

3.1. *Surface-renewal frequency*

Figure 4(*a*) shows a recording of the instantaneous value of the concentration fluctuation $c(t)$ measured at a point ($x/\delta = 22$ and $z/\delta = 0$) on the free surface ($y/\delta = 1$), where the position of the point source corresponded to $x/\delta = 0$. Very positively skewed spikes of concentration fluctuation are observed. The peak values of these concentration spikes are much larger than the mean concentration, and the ratio of the ensemble-averaged values of the peaks $\langle C_p \rangle$ to the mean concentration $\bar{C}$ reaches 6.5 at the free surface ($y/\delta = 1$) as shown in figure 5(*a*). In contrast to this

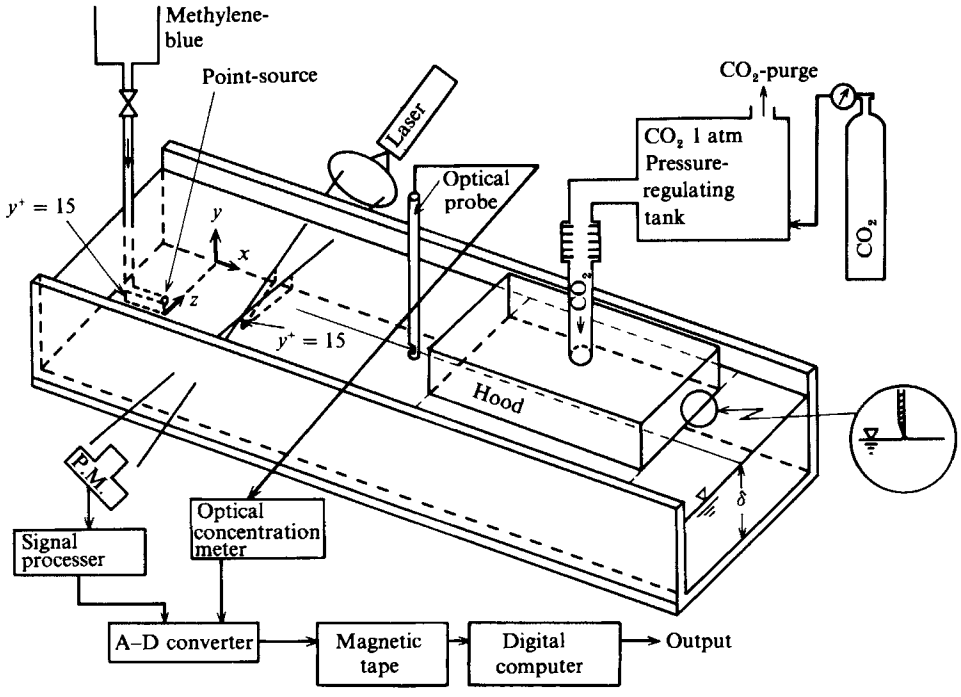

FIGURE 3. Experimental instruments and data-acquisition system.

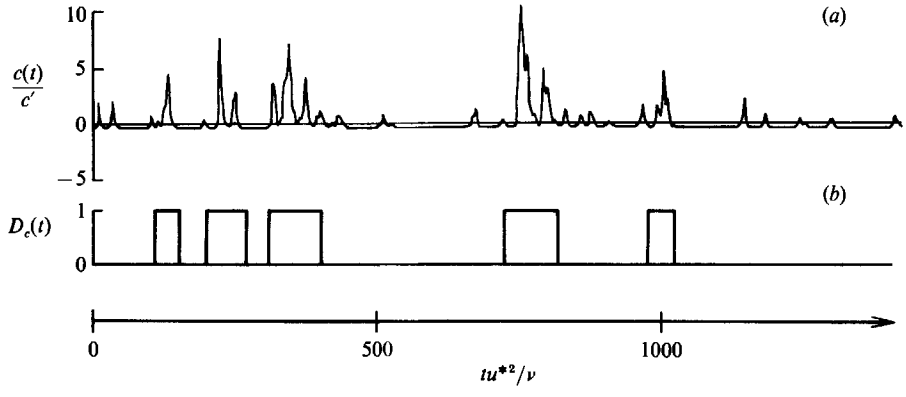

FIGURE 4. Simultaneous recordings of the instantaneous values of (*a*) $c(t)$ and (*b*) $D_c(t)$ measured at the free surface (run V; $x/\delta = 22$).

large value, the ratio of $\langle C_p \rangle$ to $\langle C_p \rangle_{y^+=15}$ at the elevation of the point source is scattered around 1.0 (figure 5*b*). These results show that the methylene-blue tracer emitted in the buffer layer is not dispersed but convected upward by the large-scale turbulent eddies, i.e. bursting eddies. This also suggests that large-scale turbulent eddies approach the free surface from the buffer region (around $y^+ = 15$) and they arrive at the free surface. This is confirmed by the streaks of methylene-blue, visualized by a video camera, which showed a trajectory of the contaminated fluid rising from the wall region toward the interfacial region. The structure of the surface-renewal eddy has been investigated in detail by Komori *et al.* (1982*a*, 1988). Using an infrared-radiative scanner and a laser-Doppler velocimeter to see the pattern of the surface-renewal eddy at the free surface and in the vicinity of it, they showed that

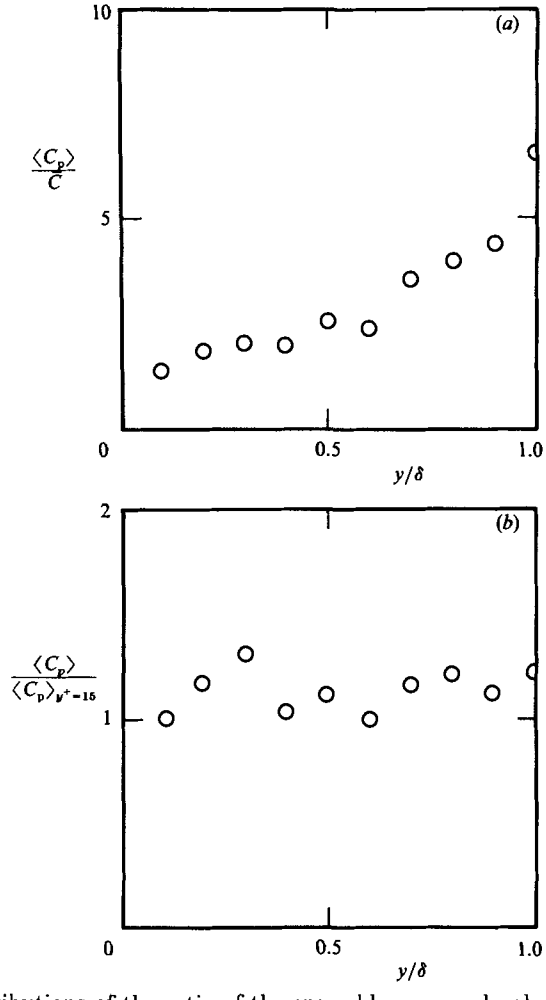

FIGURE 5. Distributions of the ratio of the ensemble-averaged values of concentration peaks $\langle C_p \rangle$ to (*a*) the mean concentration $\bar{C}$ and (*b*) $\langle C_p \rangle$ at $y^+ = 15$ (run V; $x/\delta = 22$).

the dimensions of the renewal eddy are 2δ, 0.5δ and δ in the streamwise, vertical and spanwise directions, respectively.

The surface-renewal motions may be detected using a sophisticated eduction technique for the positively skewed spikes of $c(t)$ shown in figure 4(*a*). If the renewal motions can be detected by an eduction technique, the count of the mean spikes per second will give the surface-renewal frequency f_s. Thus, in this study, the variable interval time-averaging (VITA) technique of Blackwelder & Kaplan (1976) was applied to the concentration fluctuation measured at the free surface. The variable interval time-average (VITA) for an instantaneous concentration $C(t)$ at a particular position is defined by

$$C(t, T) = \frac{1}{T}\int_{t-\frac{1}{2}T}^{t+\frac{1}{2}T} C(s)\,\mathrm{d}s, \tag{1}$$

where T is the averaging time. A localized measure of the concentration intensity is represented by the localized variance

$$\widehat{\mathrm{var}}\,(t, T) = \hat{C}^2(t, T) - [\hat{C}(t, T)]^2. \tag{2}$$

Using this variance, a detection function of concentration spikes is defined by

$$D_c(t) = \begin{cases} 1 & \text{if } \widehat{\text{var}} > kc'^2 \\ 0 & \text{otherwise} \end{cases}, \tag{3}$$

where k is the threshold level and c' is the conventional r.m.s. of $c(t)$. In addition, the number of intervals in which $D_c(t) = 1$ is assumed to give the number of surface-renewal events, $N_s(x)$.

An averaging time of $Tu^{*2}/\nu = 45$ was used here. Its value was determined to cut off the higher-frequency components of $c(t)$ rather than the frequency of typical concentration spikes, by comparing the recording of $c(t)$ with that of $D_c(t)$ at $x/\delta = 22$ where the spikes are pronounced. The threshold level k was determined by plotting the number of surface-renewal events $N_s(x)$ against k. Variations of $N_s(x)$ measured at two positions, $x/\delta = 24$ and 44, are shown in figure 6. They show a similar shape to each other and have a plateau near $k = 0.4$. Thus, the value of $k = 0.4$ was selected here to be the threshold value. The details of the choice of T and k will be discussed again in §3.2. The recording of $D_c(t)$ based on values of $Tu^{*2}/\nu = 45$ and $k = 0.4$ is shown in figure 4(*b*), together with the simultaneous recording of $c(t)$ at $x/\delta = 22$. The recordings show that the positive spikes of $c(t)$ due to surface-renewal eddies can clearly be educed by the detection function $D_c(t)$. Thus the surface-renewal frequency will be calculated by

$$f_s = N_s(x)/T_{sm}, \tag{4}$$

where T_{sm} is a sampling interval (600 s in this study).

However, in order that $N_s(x)$ gives the exact number of surface-renewal events the following three conditions are required:

(*a*) Surface-renewal eddies should not deviate appreciably in the spanwise direction over their integral scales during their passage from the buffer region to the free surface.

(*b*) When the concentration tracer is carried upward by the surface-renewal eddies, defected spots without tracer are advected downstream. Other renewal eddies arriving at the measuring point of the free surface should not be generated in the defected-spots region.

(*c*) Surface-renewal motions should be generated only in the buffer region.

In order to verify the above conditions, three preliminary experiments were done.

3.1.1. *Effect of spanwise deviation of surface-renewal eddies on* $N_s(x)$

To estimate the effect of spanwise deviation of surface-renewal eddies, another point source was mounted at dimensionless distances $z^+ = 100$ or $z^+ = 200$ from the fixed point source ($z^+ = 0$) and at the same elevation, i.e. $y^+ = 15$. These separations correspond to one and two times the mean spanwise spacing $z^+ = 100$ between upward-ejected motions (low-speed streaks) given by Smith & Metzler (1983) and Komori, Murakami & Ueda (1989). Only if the surface-renewal eddies deviate significantly in the spanwise direction, i.e. outside the range of integral scales of the surface-renewal eddies, will $N_s(x)$ measured at $z^+ = 0$ on the free surface differ when one or two sources are used. Figure 7 shows the variation of $N_s(x)$ with the number of sources and the position of the second source. The distribution of $N_s(x)$ does not change among the three experiments and $N_s(x)$ always reaches a constant maximum value in the region of $x/\delta > 35$, as shown by a dashed line. This supports condition (*a*), that the surface-renewal eddies rising from the buffer region do not deviate appreciably in the spanwise direction during their passage, and it also shows that the

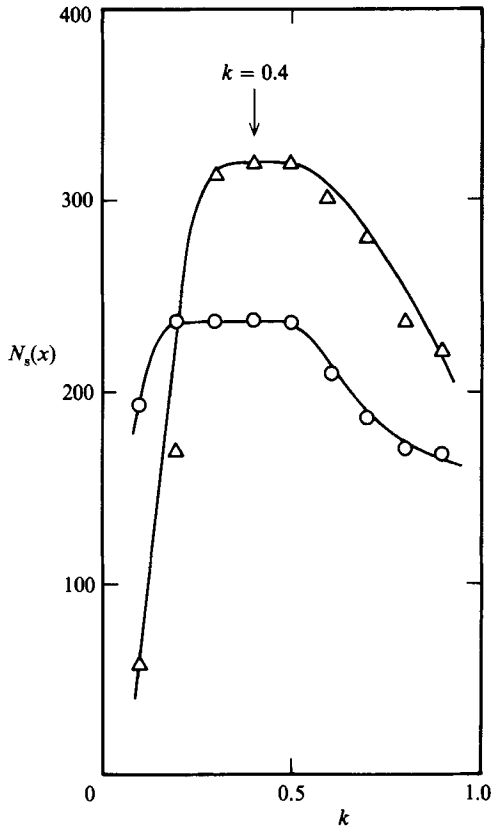

FIGURE 6. Profiles of the number of surface-renewal events with a threshold level k (run V): ○, $x/\delta = 22$; △, $x/\delta = 44$. Lines show best-fit curves.

counting errors in $N_s(x)$ due to the spanwise deviation of the surface-renewal eddies are negligibly small.

3.1.2. *Effect of tracer defect of a point-source on* $N_s(x)$

Some concentration-defected spots are generated by the rising surface-renewal eddies in the buffer layer downstream from the point source, and they are advected downstream. Even if other renewal eddies which originate in the downstream region pass into the defected spots and then arrive at the measuring point of the free surface, they cannot be counted as surface-renewal eddies because of the eddies without tracer. In order to carefully check this effect due to the tracer defect of a point source, a further point source was placed at the two downstream positions of ($x^+ = 3400$ [$x/\delta = 10$], $y^+ = 15$) and ($x^+ = 6800$ [$x/\delta = 20$], $y^+ = 15$), in addition to the fixed point source located at a point of ($x^+ = 0$ and $y^+ = 15$). The streamwise distance of $x^+ = 3400$ corresponded roughly to 34 times the overall length of the ejecting eddies (low-speed streaks) in the buffer region (Smith & Metzler 1983). Figure 8 compares $N_s(x)$ when a second source at different streamwise distances is used. $N_s(x)$ does not change significantly among the three experiments, and the two-source experiments give the same constant maximum value at large x/δ as those for one source. This fact, together with the results from figure 7, shows that a fixed point source has the same effect as a plane source located at $y^+ = 15$, and a constant

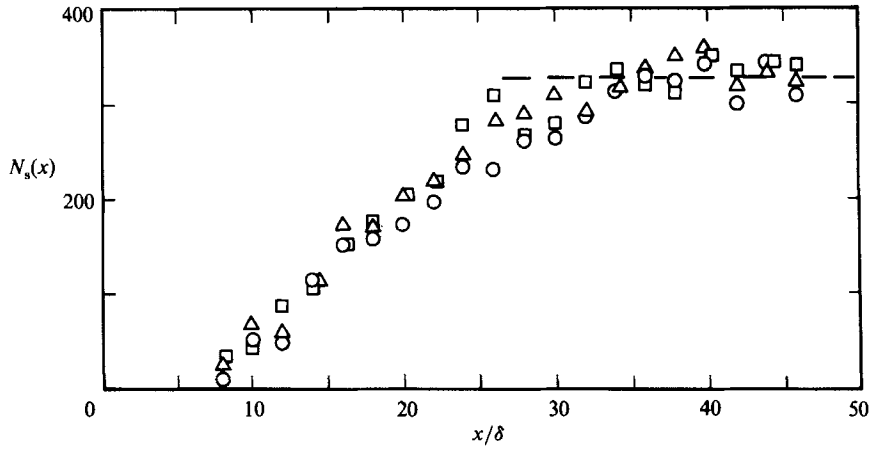

FIGURE 7. Variation of $N_s(x)$ with the number of sources and position in the spanwise direction (run V): ○, one point source ($z^+ = 0$); △, two point sources ($z^+ = 0$ and 100): □, two point sources ($z^+ = 0$ and 200). A dashed line shows the constant maximum value of $N_s(x)$ that is reached.

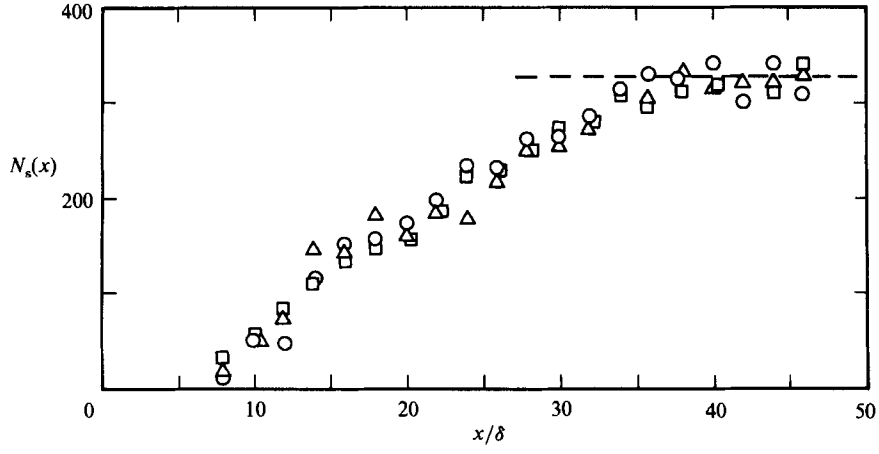

FIGURE 8. Variation of $N_s(x)$ with the number of sources and position in the streamwise direction (run V): ○, one point source ($x^+ = 0$); △, two point sources ($x^+ = 0$ and 3400); □, two point sources ($x^+ = 0$ and 6800). A dashed line shows the constant value of $N_s(x)$ that is reached.

maximum value of $N_s(x)$ gives the exact number of surface-renewal eddies that originate in the buffer region and cross the line of $z^+ = 0$ and $y^+ = 15$.

3.1.3. *Effect of surface-renewal eddies generated outside the buffer layer*

If surface-renewal eddies are generated outside the buffer by any interaction between the bursting and main flow, $N_s(x)$ obtained by a one-source experiment cannot give the total number of surface-renewal eddies arriving at the free surface. Whether surface-renewal eddies are generated outside the buffer region can be confirmed by mounting a further point source at a higher elevation in the region outside $y^+ = 15$. If surface-renewal motions are generated outside the buffer layer, $N_s(x)$ for the two-source experiments will be more than that for the one-source experiment in the downstream region where $N_s(x)$ for the one-source experiment approaches a constant maximum value. However, figure 9 shows that $N_s(x)$ for the

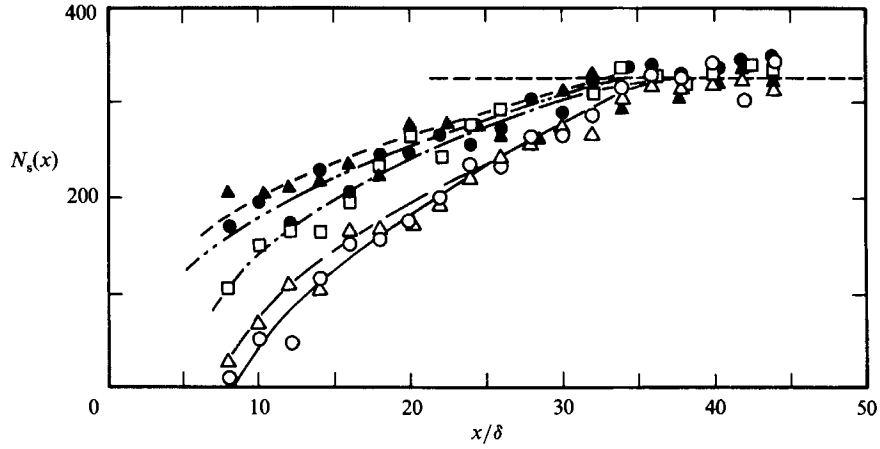

FIGURE 9. Variation of $N_s(x)$ with the number of sources and position in the vertical direction (run V): ○, one point source ($y^+ = 15$); △, two point sources ($y^+ = 15$ and 70); □, two point sources ($y^+ = 15$ and 140); ●, two sources ($y^+ = 15$ and 210); ▲, two point sources ($y^+ = 15$ and 280). Lines show best-fit curves.

two-source experiments with the second source at different elevations approaches the same constant value in the region of $x/\delta > 35$ as that of the one-source experiment. This means that surface-renewal motions always originate in the buffer region and are not generated by any interaction outside the buffer layer. The reason why $N_s(x)$ for the two-source experiments is larger than that for one source in the region of $x/\delta < 35$ can easily be understood by considering surface-renewal motions that originate in the region upstream of a fixed source.

Thus, all the conditions required in (4) were verified and so the surface-renewal frequency f_s can be estimated by substituting a constant maximum value of $N_s(x)$ in the downstream region of $x/\delta > 35$ into (4).

3.2. *Bursting frequency*

The same VITA technique as used for the detection of surface-renewal motions was applied to the instantaneous streamwise velocity $U(t)$ to educe bursting events. Substituting $U(t)$ for $C(t)$ in (1) and (2), a detection function for bursting is then defined by

$$D_u(t) = \begin{cases} 1 & \text{if } \hat{\text{var}} > ku'^2 \\ 0 & \text{otherwise} \end{cases}, \tag{5}$$

where u' is the r.m.s. of the streamwise velocity fluctuation $u(t)$. In contrast to the measurements of surface-renewal frequency, bursting frequency can be determined directly by counting a number N_B of short intervals (bursting events) in which $D_u(t) = 1$, since $U(t)$ is measured at the local point $y^+ = 15$ where the bursting is most obviously generated. Thus the bursting frequency is calculated by

$$f_B = N_B/T_{sm}. \tag{6}$$

This detection technique for bursting has been verified by many investigators, and the details can be found in Blackwelder & Kaplan (1976). However, the threshold k and averaging time T significantly affect the bursting frequency detected by the VITA technique. The choice of k and T is always controversial and cannot be

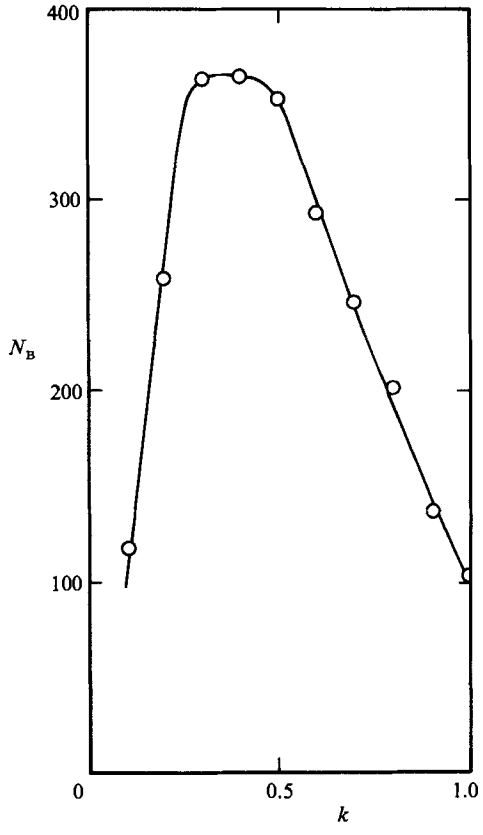

FIGURE 10. Profile of the number of bursting events with a threshold level k (run V). Line shows a best-fit curve.

justified mathematically. Blackwelder & Kaplan (1976) and Blackwelder & Haritonidis (1983) used the values of $Tu^{*2}/\nu = 10$ and $k = 1.0$–1.2 to educe bursting events in a turbulent boundary-layer flow, and many others also recommend the same values. However, Bogard & Tiederman (1986) have shown from comparisons with flow visualization that $Tu^{*2}/\nu = 26$ and $k = 0.64$ are the optimum values for the VITA technique. The values $Tu^{*2}/\nu = 10$ and $k = 1.0$ were also used in this study, but the detected bursting frequency strongly depended on the threshold value k in the case of $Tu^{*2}/\nu = 10$. That is, a plateau such as shown in figure 6 could not be observed for any k. This may be attributed to the fact that the amplitudes of the bursting signals are not always constant and they vary depending on which part of the bursting eddy is detected. Therefore, a simple sine-wave model, see the Appendix, was adopted to search for an appropriate value of T. The numerical calculations by the model showed that an averaging time comparable with the duration of a bursting event should be recommended. The bursting duration of the present flows was estimated from the time records of $u(t)$ to be roughly $45\nu/u^{*2}$ as shown in figure 16(a) of the Appendix. Therefore, this value was used here as an averaging time T, and for this averaging time, the profile of N_B has a clear plateau around $k = 0.4$ as shown in figure 10, as in figure 6. The profile of N_B is similar to that obtained by the sine-wave model shown in figure 17 of the Appendix. Thus, the values of $T = 45\nu/u^{*2}$ and $k = 0.4$ were also selected as the averaging time and

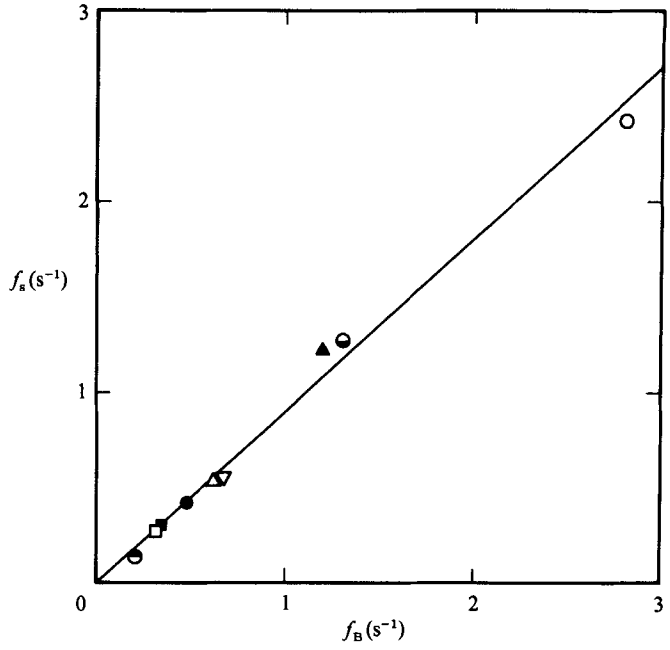

FIGURE 11. Correlation between surface-renewal frequency and bursting frequency. The line shows (7). Symbols as in table 1.

threshold level, as in the $C(t)$ case. These values are closer to the values of Bogard & Tiederman (1986) than those of Blackwelder & Haritonidis (1983) and others.

4. Results and discussion

4.1. *Correlation between f_s and f_B*

A relationship between surface-renewal motions and bursting motions can be presumed from the correlation between the surface-renewal frequency f_s and the bursting frequency f_B, since the surface-renewal motions always originate in the buffer region, as shown in §3.1.3. If the correlation is high and f_s is proportional to f_B, it can be presumed that surface-renewal motions originate during bursting. That is, bursting eddies that are generated in the buffer region are strongly lifted up towards the free surface (Komori *et al.* 1989) and arrive at the free surface. Figure 11 shows the relation between f_s and f_B under all experimental conditions listed in table 1. The correlation between f_s and f_B is extremely high, and is given by

$$f_s = 0.9 f_B. \tag{7}$$

This shows that surface-renewal motions originate in the bursting phenomena in the buffer layer, and that surprisingly almost all the (upward) ejecting eddies that are generated by bursting in the buffer region become surface-renewal eddies. This result is well supported by the fact that the surface-renewal eddies are generated only in the buffer layer (see figure 9 in §3.1.3.). Sequential pictures of the concentration streaks visualized by a video camera also suggest that surface-renewal eddies are generated by bursting in the buffer region. To strictly demonstrate the one-to-one correspondence between surface-renewal and bursting events, we must trace all the trajectories of the visualized concentration streaks that occur on the (x, z)-plane at

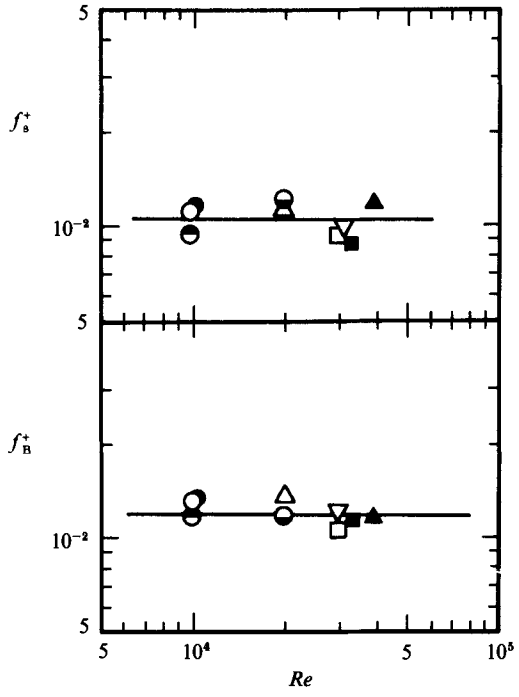

FIGURE 12. Frequencies of surface renewal and bursting, scaled with the wall variables ν and u^*, versus Reynolds number. Lines show best-fit curves. Symbols as in table 1.

$y^+ = 15$ and arrive at a measuring point on the free surface, by using a Lagrangian technique such as an image-processing method. However, all of the visualized streaks are not clear, so that these Lagrangian measurements may give large errors in counting the one-to-one correspondence. In addition, such measurements are always extremely complex and expensive, and it is almost impossible to exactly count the surface-renewal events. Therefore, the present detecting method of the surface-renewal events was devised in place of the Lagrangian detecting method.

The above results for the correlation between f_s and f_B differ somewhat from those of Jackson (1976) in that only vigorous bursting eddies (about 65% of the total) arrive at the free surface. The difference seems to be because Jackson did not measure the bursting frequency but used scaling relations obtained by other investigators in laboratory experiments, as mentioned in the introduction.

4.2. *Reynolds-number dependencies of f_s and f_B*

It is well known that the dimensionless bursting frequencies scaled with the wall and outer flow variables are well correlated with the Reynolds number Re in turbulent boundary-layer flows (Blackwelder & Haritonidis 1983; Kim, Kline & Reynolds 1971; Rao, Narashimha & Narayanan 1971). However, the influence of the Reynolds number on the bursting frequency f_B has not been clarified for open-channel flow. Thus both bursting and surface-renewal frequencies were scaled with the wall and outer flow variables, and their Reynolds-number dependencies were investigated.

Figure 12 shows frequencies of both surface renewal and bursting, scaled with the wall variables ν and u^*, versus Reynolds number. Although the dimensionless frequencies, $f_s^+ (= f_s \nu/u^{*2})$ and $f_B^+ (= f_B \nu/u^{*2})$, are lightly scattered, it is found that

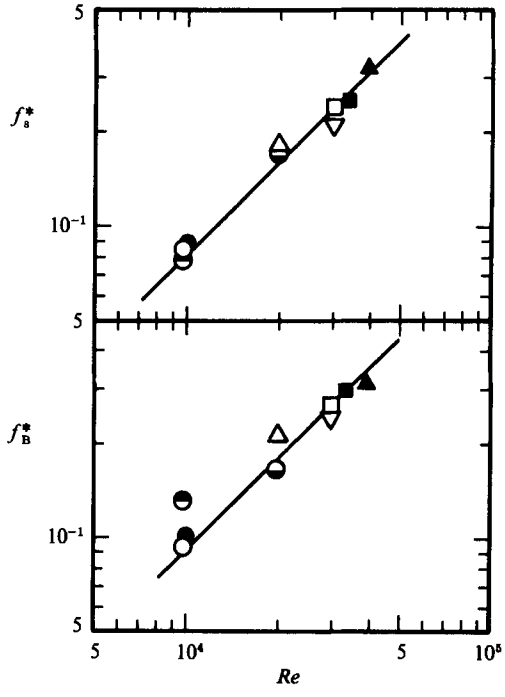

FIGURE 13. Frequencies of surface renewal and bursting, scaled with the outer flow variables δ and U_{suf} versus Reynolds number. Lines show (8). Symbols as in table 1.

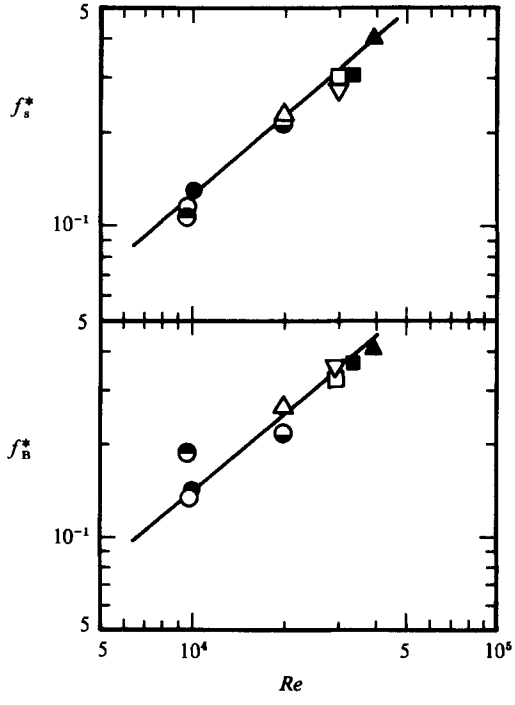

FIGURE 14. Frequencies of surface renewal and bursting, scaled with the outer flow variables δ and U_{ave} versus Reynolds number. Lines show (9). Symbols as in table 1.

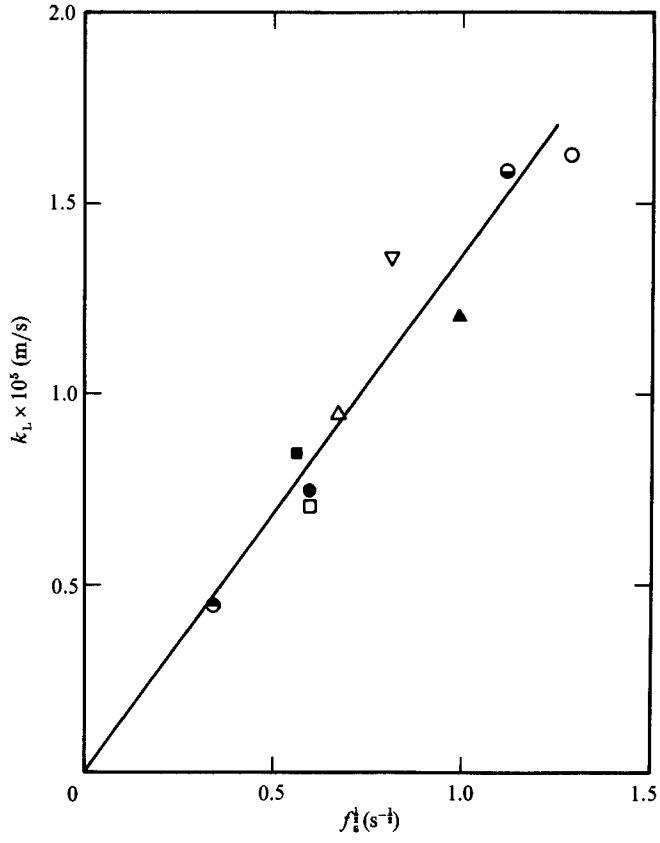

FIGURE 15. Correlation between surface-renewal frequency and mass-transfer coefficient of CO_2 on the liquid side. The line shows a best-fit curve. Symbols as in table 1.

both f_s^+ and f_B^+ are approximately constant over the Reynolds-number range. The independence of Re is in agreement with other measurements of f_B^+ in turbulent boundary-layer flows (Blackwelder & Haritonidis 1983; Chambers, Murphy & McEligot 1983).

Dimensionless frequencies, $f_s^*(=f_s\delta/U^0)$ and $f_B^*(=f_B\delta/U^0)$, scaled with the outer flow variables δ and U^0, are shown in figures 13 and 14, where the characteristic velocity U^0 is U_{suf} or U_{ave}. Frequencies of both surface renewal and bursting scaled with the outer flow variables increase with increasing Re, and they are well correlated with the Reynolds numbers. The Reynolds-number dependencies are given by

$$f_s^* = 0.9f_B^* = \begin{cases} 9.3\times10^{-6}Re^{0.983} & \text{for } U^0 = U_{suf}, \quad (8) \\ 4.7\times10^{-5}Re^{0.854} & \text{for } U^0 = U_{ave}. \quad (9) \end{cases}$$

The increase in the dimensionless frequencies scaled with outer flow variables is also in agreement with the results obtained in a turbulent boundary layer (Blackwelder & Haritonidis 1983; Rao *et al.* 1971). In particular, the correlation equation (8) scaled with δ and U_{suf} shows that the frequencies have a strong proportionality to U_{suf}. This supports the Komori *et al.*'s (1982*a*) assumption that the surface-renewal frequency has a strong proportionality to the mean free-surface velocity.

4.3. *Effects of surface-renewal motions on mass transfer across the free surface*

Figure 15 shows the correlation between the surface-renewal frequency f_s and the mass-transfer coefficient on the liquid side, k_L, under all the experimental conditions listed in table 1. It is found that the measured k_L is clearly proportional to the square root of f_s. Its proportionality follows the surface-renewal theory of Dankwerts (1951), and shows that the mass transfer across the free surface is dominated by the large-scale surface-renewal motions discussed in §4.2. This also validates the present detection technique for the surface-renewal eddies.

The next step of this study is to develop a model of heat and mass transfer across a gas–liquid interface. The results obtained from figure 15 suggest that a surface-renewal model, including both the Reynolds-number dependencies and the effects of the wall or the outer flow variables shown in figures 12, 13 and 14, may be quite useful in estimating the turbulent heat and mass transfer across a gas–liquid interface.

5. Summary

The relationship between surface-renewal motions and bursting motions has been investigated experimentally through mass-transport experiments using a point source in an open-channel flow, and the effects of the surface-renewal motions on the mass transfer across the free surface were examined by CO_2-absorption experiments. The main results from this study can be summarized as follows.

(1) Surface-renewal motions that appear in the interfacial region are inferred to originate in bursting phenomena in the buffer region. That is, it is deduced that large-scale turbulent eddies ejected by bursting rise from the buffer region towards the interfacial (outer) region and arrive at and renew the free surface.

(2) Frequencies of both surface renewal and bursting detected by the VITA technique are determined uniquely by the wall variables or the outer-flow variables and the Reynolds number.

(3) Mass transfer across the free surface is dominated by the large-scale surface-renewal motions. The mass-transfer coefficient on the liquid side is proportional to the square-root of the surface-renewal frequency, that is, it follows the surface-renewal theory of Dankwerts (1951).

To directly confirm the above relationship between the surface renewal and bursting motions, the development of a more sophisticated technique may be required to trace all the trajectories of the bursting eddies originating at a local point in the buffer layer. The averaging time and threshold level used in the present VITA technique may be controversial and a more reliable detecting technique for the numbers of bursting and surface-renewal events may be desired. Furthermore, it should be noted that all of the above results may not be applicable to such geophysical flows as rivers, because the flow depth and Reynolds number of the present flow are extremely small compared with geophysical flows and it is not clear whether the bursting events exist in such geophysical flows. However the present results may be of immense practical importance in estimating heat and mass transfer across the gas–liquid interfaces of flows in industrial equipment related to absorption and evaporation.

The authors gratefully acknowledge financial support for this research provided by the Nissan Science Foundation, Harada Memorial Foundation and Japanese Ministry of Education under Grant No. 63550712. They also thank Mr Yosiyuki Hiraga for his

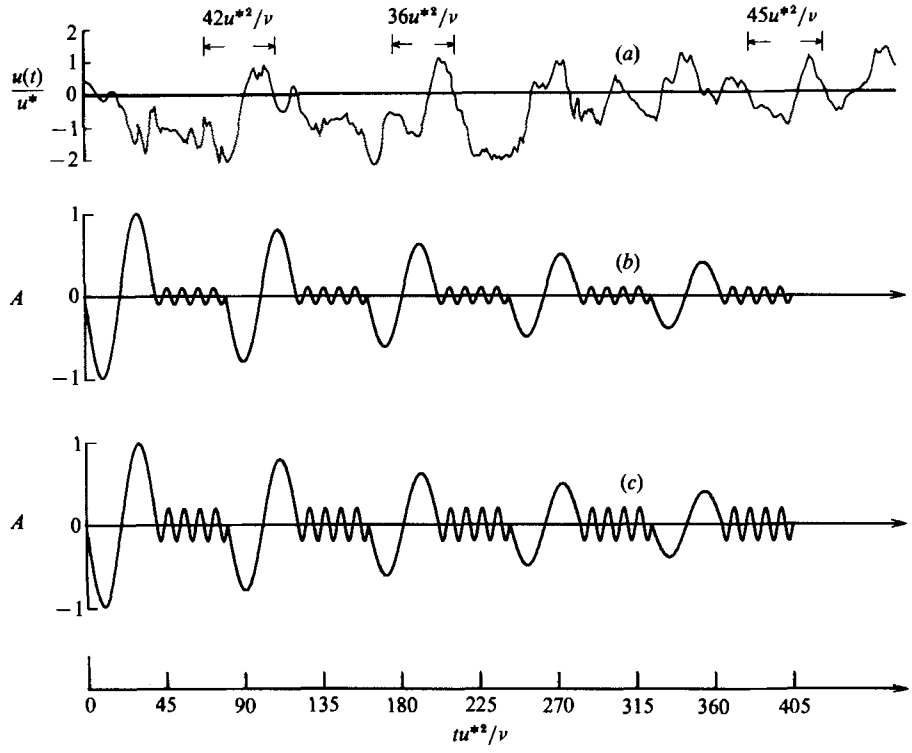

FIGURE 16. Time records of the streamwise velocity fluctuations $u(t)$ (run V) and sine waves used as model signals of bursting: (*a*) $u(t)$; (*b*) sine wave with interval $90\nu/u^{*2}$ and $B = 0.1$; (*c*) sine wave with interval $90\nu/u^{*2}$ and $B = 0.2$.

great help in conducting experiments, Professor I. Nezu for helpful discussion on flow structure of a geophysical flow and Professor R. F. Blackwelder for providing an original programme for the VITA technique.

Appendix. An averaging time T and a threshold level k

The bursting duration can roughly be estimated as $45\nu/u^{*2}$ from a time record of the streamwise velocity fluctuation $u(t)$ as shown by arrows in figure 16(*a*). Similarly we can see duration values of about $25\nu/u^{*2}$ from figure 3 of Johansson & Alfredsson (1982) and about $64\nu/u^{*2}$ from figure 7 of Blackwelder & Kaplan (1976). The present duration of $45\nu/u^{*2}$ lies between these latter two. Also, the results in figure 12 show that the interval between the bursting events is close to $90\nu/u^{*2}$ and it corresponds to double the bursting duration. Blackwelder & Haritonidis (1983) proposed the longer interval of $300\nu/u^{*2}$. Thus, we assume a simple model of the streamwise velocity fluctuation as follows:

(1) The bursting signals can be approximated by the sine waves $u(t) = -A\sin(2\pi u^{*2}t/45\nu)$ with five amplitudes of $A = 0.4, 0.5, 0.6, 0.8$ and 1.0 and a period of $45\nu/u^{*2}$, as shown in figure 16(*b*, *c*), since the bursting signals never have the same amplitudes. The sine waves appear successively at an interval of $90\nu/u^{*2}$ or $300\nu/u^{*2}$, and the duration of the sine waves is equal to $45\nu/u^{*2}$.

(2) High frequency-sine waves $u(t) = -B\sin(2\pi u^{*2}t/10\nu)$ with a small amplitude

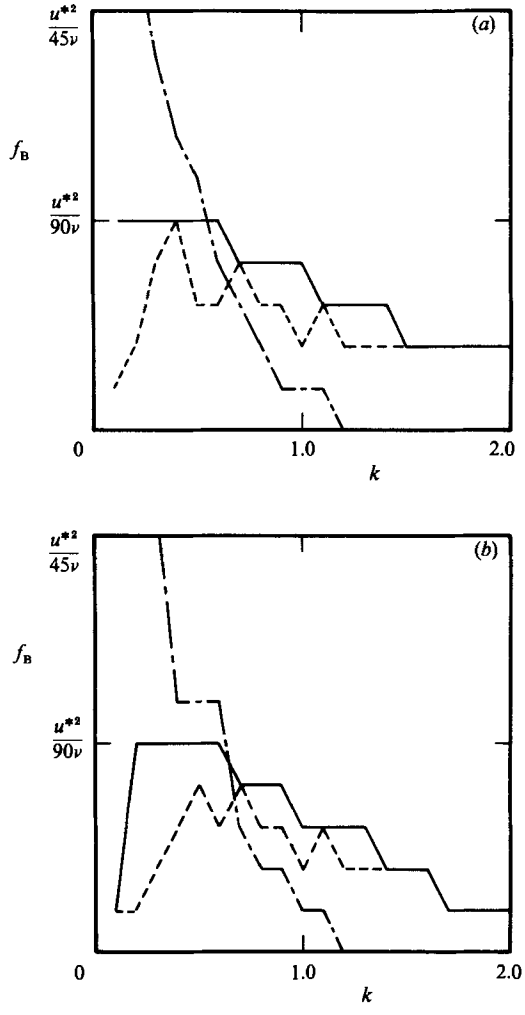

FIGURE 17. Bursting frequency predicted by a sine-wave model with interval $90\nu/u^{*2}$ versus threshold level k: (*a*) $B = 0.1$; (*b*) $B = 0.2$; —·—·—, $T = 10.0\nu/u^{*2}$; ——, $T = 45.0\nu/u^{*2}$; – – – –, $T = 67.5\nu/u^{*2}$.

of $B = 0.1$ or 0.2 and a period of $10\nu/u^{*2}$ always appear between bursting events, as shown in figure 16(*b*, *c*), irrespective of the bursting.

Of course, more complicated waves may be proposed, but the results obtained may be very similar to those from the above simple wave model. When the VITA technique is applied to the model signals shown in figures 16(*b*, *c*), the detected bursting frequencies for the two intervals of $90\nu/u^{*2}$ and $300\nu/u^{*2}$ shown in figures 17 and 18 are obtained, as a function of threshold level k in increments of 0.1. The right bursting frequency detected should be, of course, equal to the inverse of the interval. The figures show that only curves with the same averaging time $T = 45\nu/u^{*2}$ as the bursting duration can give the right detection of the bursting frequency in the range of $k = 0.4$–0.6. The results also suggest that the averaging time T in the VITA technique should be chosen as the bursting duration and a threshold level of $k = 0.4$ is appropriate.

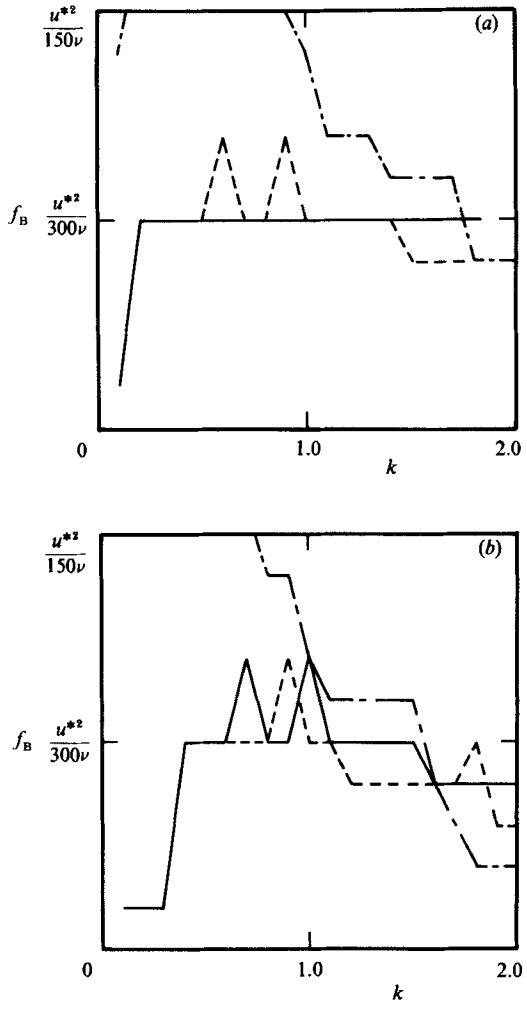

FIGURE 18. Bursting frequency predicted by a sine-wave model with interval $300\nu/u^{*2}$ versus threshold level k: (a) $B = 0.1$; (b) $B = 0.2$; ——·——, $T = 10.0\nu/u^{*2}$; ——, $T = 45.0\nu/u^{*2}$; – – – –, $T = 67.5\nu/u^{*2}$.

REFERENCES

BLACKWELDER, R. F. & HARITONIDIS, J. H. 1983 Scaling of the bursting frequency in turbulent boundary layers. *J. Fluid Mech.* **132**, 87–103.

BLACKWELDER, R. F. & KAPLAN, R. E. 1976 On the wall structure of the turbulent boundary layer. *J. Fluid Mech.* **76**, 89–112.

BOGARD, D. G. & TIEDERMAN, W. G. 1986 Burst detection with single-point velocity measurements. *J. Fluid Mech.* **162**, 389–413.

CHAMBERS, F. W., MURPHY, H. D. & MCELIGOT, D. M. 1983 Laterally converging flow. Part 2. Temporal wall shear stress. *J. Fluid Mech.* **127**, 403–428.

DANKWERTS, P. V. 1951 Significance of liquid-film coefficients in gas absorption. *Ind. Engng Chem.* **43**, 1460–1467.

HUNT, J. C. R. 1984 Turbulence structure and turbulent diffusion near a gas–liquid interface. In *Gas Transfer at Water Surfaces* (ed. W. Brutsaert & G. H. Jirka), pp. 67–82. Reidel.

JACKSON, R. G. 1976 Sedimentological and fluid-dynamic implications of the turbulent bursting phenomenon in geophysical flows. *J. Fluid Mech.* **77**, 531–560.

JOHANSSON, A. V. & ALFREDSSON, P. H. 1982 On the structure of turbulent channel flow. *J. Fluid Mech.* **122**, 295–314.

KIM, H. T., KLINE, S. J. & REYNOLDS, W. C. 1971 The production of turbulence near a smooth wall in a turbulent boundary layer. *J. Fluid Mech.* **50**, 133–160.

KOMORI, S., HIRAGA, Y., MURAKAMI, Y. & UEDA, H. 1988 The generation of surface renewal eddies in an open-channel flow. In *Proc. 2nd Intl Symp. on Transport Phenomena in Turbulent Flows*, (ed. M. Hirata & N. Kasagi), pp. 213–223. Hemisphere.

KOMORI, S., MURAKAMI, Y. & UEDA, H. 1989 Detection of coherent structures associated with bursting events in an open-channel flow by a two-point LDV-measuring technique. *Phys. Fluids* A **1**, 339–348.

KOMORI, S. & UEDA, H. 1985 The large-scale coherent structure in the intermittent region of the self-preserving round free jet. *J. Fluid Mech.* **152**, 337–359.

KOMORI, S., UEDA, H., OGINO, F. & MIZUSHINA, T. 1982*a* Turbulent structure and transport mechanism at the free surface in an open-channel flow. *Intl J. Heat Mass Transfer* **25**, 513–521.

KOMORI, S., UEDA, H., OGINO, F. & MIZUSHINA, T. 1982*b* Lateral and longitudinal turbulent diffusion of scalar quantities in thermally stratified flow in an open channel. In *Proc. Seventh Intl Heat Transfer Conf.* (ed. U. Grigull, E. Hahne, K. Stephan & J. Straub), vol. 2, pp. 431–436. Hemisphere.

MIZUSHINA, T., OGINO, F., UEDA, H. & KOMORI, S. 1978 Buoyancy effects on eddy diffusivities in thermally stratified flow in an open channel. In *Proc. of Sixth Intl Heat Transfer Conf.* (ed. J. T. Rogers), vol. 1, pp. 91–96. Hemisphere.

RAO, K. N., NARASHIMHA, R. & NARAYANAN, M. A. B. 1971 The bursting phenomenon in a turbulent boundary layer. *J. Fluid Mech.* **48**, 339–352.

SMITH, C. R. & METZLER, S. P. 1983 The characteristics of low-speed streaks in the near-wall region of a turbulent boundary layer. *J. Fluid Mech.* **129**, 27–54.